Effect of La doping on the ferroic order in Pb-based perovskite-type relaxor ferroelectrics

B. J. Maier,[1,*] A.-M. Welsch,[1,2] B. Mihailova,[1,†] R. J. Angel,[1,3] J. Zhao,[3] C. Paulmann,[1] J. M. Engel,[1] W. G. Marshall,[4] M. Gospodinov,[5] D. Petrova,[6] and U. Bismayer[1]

[1]*Department Geowissenschaften, Universität Hamburg, Grindelallee 48, D-20146 Hamburg, Germany*

[2]*Institut für Mineralogie, Leibniz Universität Hannover, Callinstrasse 3, D-30167 Hannover, Germany*

[3]*Virginia Tech Crystallography Laboratory, Department of Geosciences, Virginia Tech, Blacksburg, Virginia 24060, USA*

[4]*ISIS Neutron Facility, STFC Rutherford Appleton Laboratory, Harwell Science and Innovation Campus, Harwell Oxford, Chilton, Oxon OX11 0QX, United Kingdom*

[5]*Institute of Solid State Physics, Bulgarian Academy of Sciences, Blvd. Tzarigradsko Chausse 72, 1784 Sofia, Bulgaria*

[6]*South-West University "Neofit Rilski," 66 Ivan Mihailov Strasse, 2700 Blagoevgrad, Bulgaria*

(Received 16 January 2011; published 7 April 2011)

The structural alteration induced by the substitution of three-valent cations with an isotropic electronic outermost shell for Pb^{2+} in perovskite-type relaxors was investigated in the solid solutions $Pb_{1-x}La_xSc_{(1+x)/2}Ta_{(1-x)/2}O_3$, $x = 0.08$ (PST-La) and $Pb_{1-x}La_xSc_{(1+x)/2}Nb_{(1-x)/2}O_3$, $x = 0.23$ (PSN-La). In order to distinguish the "charge" effects from "strain" effects associated with the incorporation of La^{3+} in the structure, Sr-containing $PbSc_{0.5}Nb_{0.5}O_3$ was characterized as well. The structure of the compounds was analyzed by *in situ* Raman spectroscopy, single-crystal x-ray diffraction, and powder neutron diffraction at different temperatures or pressures. It is shown that the embedding of La^{3+} strongly affects the ferroic structural species due to strain effects through a disturbance of the system of lone-pair electrons associated with Pb^{2+} and a decrease in the tolerance factor. La doping suppresses the dynamical coupling between off-centered Pb and *B*-site cations and enhances antiphase BO_6 octahedral tilting which, depending on the level of doping, may lead to long-range order of antiphase BO_6 tilts at ambient conditions and frustrated antiferroelectric order of Pb ions at low temperatures.

DOI: 10.1103/PhysRevB.83.134106 PACS number(s): 61.50.Ks, 64.70.Nd, 77.80.Jk, 78.30.−j

I. INTRODUCTION

Relaxor ferroelectrics with the perovskite-type (ABO_3) structure are technologically important materials with multiple structural and chemical inhomogeneities, whose structural peculiarities have been challenging solid-state scientists for a long time.[1–3] Relaxors are characterized by the existence of a broad, frequency-dependent peak of the dielectric permittivity as a function of temperature. The remarkably strong dielectric, piezoelectric, pyroelectric, electroelastic, and optoelectric responses of relaxor compounds are closely related to the existence of nanosized spatial regions having local polarizations that flip over several different orientational states, which are equivalent under the crystallographic symmetry of the surrounding cubic matrix.[2,3] These polar nanoregions (PNRs) are formed at the Burns temperature T_B,[4] which is usually several hundred Kelvin above the temperature of the dielectric permittivity peak T_m. At an intermediate temperature T^* between T_B and T_m the preexisting PNRs enlarge and their reorientation rate slows down;[5–8] the coupling is realized mainly via enhanced coherence of the off-centered displacements of the *B*-site cations[6] and is strongest along the cubic ⟨110⟩ directions.[9] Below T_m some relaxors undergo a para-to-ferroelectric phase transition with a rather weak ferroelectric distortion of the unit cell. For canonical relaxors the PNRs persist down to very low temperatures, without merging into long-range ordered ferroelectric domains, but PNRs become static at the freezing temperature $T_f < T_m$.[2] Under pressure Pb-based relaxors undergo a continuous phase transition from a cubic to a rhombohedral structure, involving the development of long-range order of antiphase octahedral tilts, local ferroic order of the Pb atoms, and a suppression of the off-centered displacements of the *B*-site cations.[10–15] The critical pressure at which the symmetry of the global structure is broken is preceded by a characteristic intermediate pressure p^* at which the existing off-centered Pb and *B*-site cations dynamically decouple and antiphase octahedral tilt order is detectable by neutron diffraction.[10,11,14,15]

The reason for the appearance of PNRs at high temperatures and the suppression of ferroelectric order at low temperatures is still under discussion. It is widely accepted that the relaxor state in perovskites is due to charge imbalance and corresponding local random electric fields associated with the compositional disorder on the cation sites. The underlying idea of this theoretical model is based on the experimentally observed correlation between the degree of chemical order on the *B* site and the relaxor-to-normal ferroelectric crossover.[16] An alternative concept is that random elastic fields due to local distortions and/or mismatch of different ionic radii are the more plausible and universal explanation of the relaxor state, since it is applicable even to relaxors with no chemical disorder such as $Cd_2Nb_2O_7$.[17] This model is strongly supported by recent comparative studies on the temperature- and pressure-induced structural transformations in Ba- and Bi-doped $PbSc_{0.5}Nb_{0.5}O_3$ (PSN) relaxors.[11,13,18] Ba^{2+} and Bi^{3+} doping represent, correspondingly, homovalent and heterovalent substitution for Pb^{2+} on the *A* site of the perovskite structure, i.e., only Bi^{3+} doping induces local electric fields. In addition, due to the ionic-radius difference $[r_i(Ba^{2+}) = 1.61\ Å > r_i(Pb^{2+}) = 1.49 \geqslant r_i(Bi^{3+}) = 1.45]$[19,20] and the shape of the outermost electron shell (isotropic for Ba^{2+}, stereochemically active lone pair for both Pb^{2+} and Bi^{3+}), Ba^{2+} incorporation induces strong local elastic-stress fields inside the structure, whereas the embedding of Bi^{3+} barely affects the local structure. Combined x-ray diffraction

(XRD) and Raman spectroscopic analyses revealed that the substitution of Ba^{2+} for Pb^{2+} suppresses the development of ferroic long-range order (ferroelectric type on cooling,[1–3] antiferrodistortive type under pressure[14,15]), whereas Bi^{3+} enhances the fraction of the ferroic phase developing on temperature decrease as well as on pressure increase. This suggests that the elastic fields induced by compositional disorder may be a very important factor for the occurrence of a relaxor state. Furthermore, first-principles calculations on Ba-based relaxor ferroelectrics with homovalent *B*-site substitution with the dopant ionic radius being larger than the radius of the dominant *B* cation clearly demonstrated the relationship between the size difference of the *B*-site cations and the local structural strains.[21]

So far, however, the possible size effects associated with heterovalent substitution have not been considered. For example, it is well known that La doping of $PbZr_{1-x}Ti_xO_3$ leads to a crossover from a normal ferroelectric to a relaxor state,[22–25] but this always has been attributed to the doping-induced local electric fields. To elucidate whether the difference in the ionic radii is significant for the type of ferroic state in the case of heterovalent substitution, we chose to analyze La-doped $PbSc_{0.5}Ta_{0.5}O_3$ (PST) and PSN. The substitution of La^{3+} for Pb^{2+} can affect the structure of relaxors in several ways: (i) it introduces local electric fields due to the valence difference; (ii) it may induce Pb vacancies and variations in stoichiometry on the *B* site, when the *B* site is occupied by heterovalent cations, in order to compensate the surplus charge on the *A* site; (iii) due to the smaller ionic radius of 12-coordinated $La^{3+}[r_i(La^{3+}) = 1.36\ \text{Å} < r_i(Pb^{2+}) = 1.49\ \text{Å}$ (Ref. 19)], the tolerance factor $t = r_i(A) + r_i(O)/\sqrt{2}[r_i(B) + r_i(O)]$ is reduced, which in general favors the development of BO_6 tilting; and (iv) La^{3+} has an isotropic outermost electron shell and therefore La doping disturbs the system of electron lone pairs associated with *A*-site Pb^{2+} cations. In order to discriminate the "charge" effects (the first two specified above) from the "strain" effects (the last two specified above) we also analyzed PSN doped with Sr^{2+}, since in this case the tolerance factor is also reduced due to the smaller ionic radius $[r_i(Sr^{2+}) = 1.44\ \text{Å} < r_i(Pb^{2+}) = 1.49\ \text{Å}$ (Ref. 19)] and the lone-pair coupling is disturbed, without introducing any charge imbalance in the system. The analysis of the structural changes when temperature and pressure are varied independently is helpful for developing a better understanding of the structure at ambient conditions. In this paper we present our results from XRD and Raman-scattering experiments performed at different temperatures and ambient pressure as well as at different pressures and room temperature. The structure of La-doped PSN at ambient and high pressures was also studied by powder neutron diffraction.

II. EXPERIMENTAL DETAILS

A. Single-crystal growth and chemical composition

Single crystals of La-doped PST and PSN as well as Sr-doped PSN were synthesized by the high-temperature solution crystal growth method using a flux of $PbO:PbF_2:B_2O_3$ with a ratio 0.85:0.10:0.05 and by cooling the synthesis mixture from 1200 °C to 920 °C at a rate of 0.5 °C/h.

TABLE I. Tolerance factors of the compounds studied.

	PST	PST-La		PSN	PSN-La		PSN-Sr
t	0.977	0.971[a]	0.942[b]	0.977	0.961[a]	0.926[b]	0.971

[a]Without taking into account the vacancies.
[b]Taking into account the vacancies.

Backscattered electron images (Cameca microbeam SX100 SEM system) confirmed the chemical homogeneity of the single-crystal specimens. The actual chemical composition was determined using electron microprobe analysis, by averaging over 100 spatial points. The calculated chemical formula was $Pb_{0.86}La_{0.08}\square_{0.06}Sc_{0.53}Ta_{0.47}O_{2.93}$ for the tantalate compound and $Pb_{0.70}La_{0.23}\square_{0.07}Sc_{0.62}Nb_{0.38}O_{2.93}$ for the niobate compound, which can be approximated as $Pb_{1-x}La_xSc_{(1+x)/2}Ta_{(1-x)/2}O_3$, $x = 0.08$ (PST-La) and $Pb_{1-x}La_xSc_{(1+x)/2}Nb_{(1-x)/2}O_3$, $x = 0.23$ (PSN-La), respectively. The chemical composition of the Sr-doped PSN crystals studied here is $Pb_{0.66}Sr_{0.34}Sc_{0.5}Nb_{0.5}O_3$ (PSN-Sr). Plates parallel to {100} were prepared for XRD and Raman-scattering experiments.

B. X-ray diffraction

Ground portions of each of the samples were analyzed by conventional powder XRD (Philips X'Pert diffractometer) at room temperature and ambient pressure to verify the phase purity and to estimate the overall degree of chemical *B*-site order.

Synchrotron single-crystal XRD experiments were conducted at the DESY/HASYLAB F1 beam line, using a Mar-CCD 165 detector. Room-temperature and low-temperature (open-flow liquid-N_2 cryostat Oxford Cryosystems 600) measurements on PST-La and PSN-La were performed with $\lambda = 0.4000$ Å, a sample-to-detector distance of 100 mm, a step width of 0.5° per frame, and an exposure time of 200 s; reciprocal lattice sections were reconstructed using the in-house software RASTM.[26] High-pressure experiments were conducted in diamond anvil cells of Boehler-Almax[27] and Ahsbahs[28] designs with a radiation wavelength $\lambda = 0.5000$ Å, a sample-to-detector distance of 100 mm, step width of 0.5° per frame, and an exposure time of 120 s. The pressure values were determined from the pressure-induced shift of the *R*1 photoluminescence line of ruby.[29] A mixture of methanol-ethanol with a ratio 4:1 was used as a pressure-transmitting medium, which restricted the pressure range of hydrostaticity up to 9.8 GPa.[30] Synchrotron single-crystal XRD data were collected on a pressure increase between 0.6 and 6.0 GPa.

The equations of state (EoS) at room temperature were determined from the pressure dependence of the unit-cell volume *V* measured with a Huber four-circle single-crystal diffractometer equipped with a sealed-tube source. In these experiments ETH-type diamond-anvil cells[31] and a 4:1 methanol-ethanol mixture were used. The unit-cell parameters were determined by the method of eight-position diffraction beam centering,[32] ensuring a precision in the relative volume $V(p)/V_0$ of approximately 0.0001. The pressure values were calculated from the EoS of a quartz crystal loaded with the sample, with a precision of 0.01 GPa.[33]

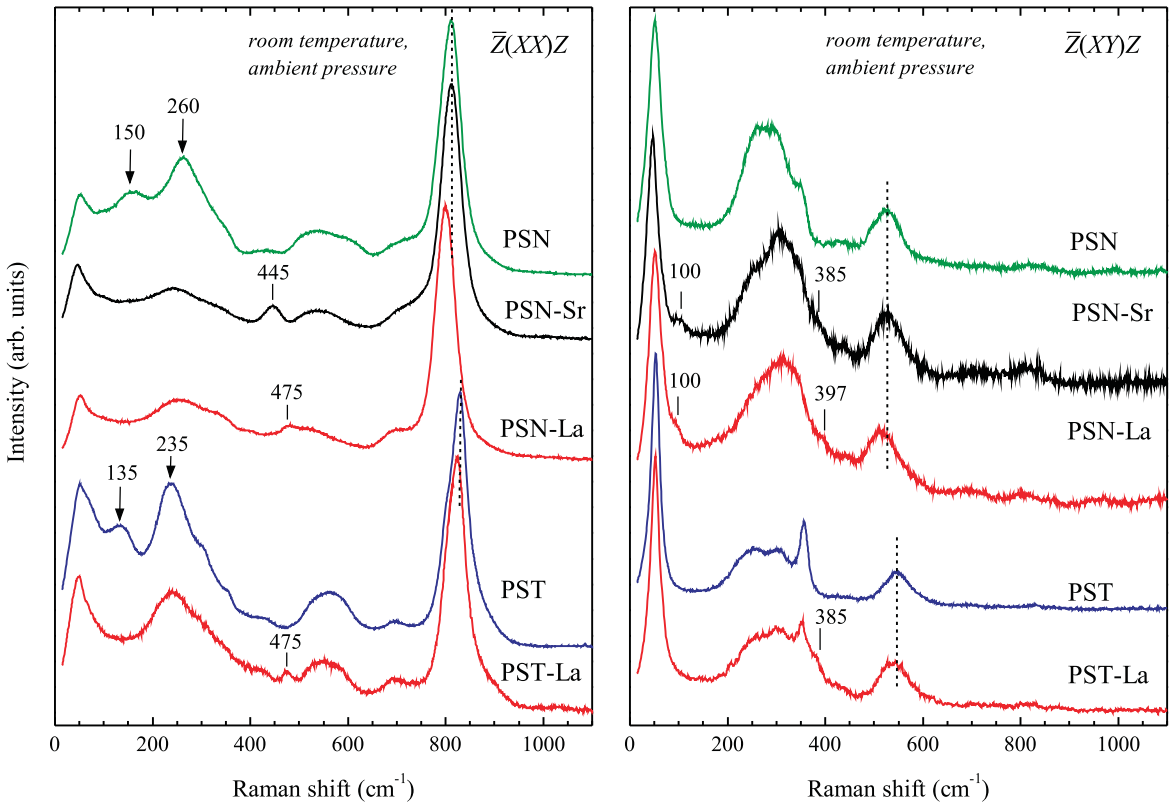

FIG. 1. (Color online) Polarized $\bar{Z}(XX)Z$ and $\bar{Z}(XY)Z$ Raman spectra of pure, Sr-, and La-doped PSN as well as pure and La-doped PST measured at 296 K and ambient pressure.

C. Neutron powder diffraction

High-pressure time-of-flight neutron powder diffraction of PSN-La was performed at PEARL, ISIS/RAL, using a Paris-Edinburgh pressure cell and a perdeuterated 4:1 methanol-ethanol mixture as the pressure-transmitting medium. Data were collected at 0, 2.03, 5.11, and 7.82 GPa with an integrated proton current of 320, 641, 643, and 881 μAh, respectively. The pressure values were determined using the EoS of PSN-La calculated from the $V(p)$ dependence measured by single-crystal XRD. A beam-line-developed correction for the wavelength and scattering-angle dependence of the neutron attenuation by the anvil (WC) and gasket (TiZr) materials was applied to the raw data. Rietveld refinements were performed with EXPGUI/GSAS,[34,35] using Bragg peak profiles consisting of a convolution of two back-to-back exponentials with a pseudo-Voigt function and a 12-term cosine Fourier series to fit the background.

D. Raman scattering

Raman spectra were collected using a Horiba Jobin-Yvon T64000 triple-grating spectrometer equipped with an Olympus BH41 microscope and a 50× long-working distance objective. The measurements were conducted in a backscattering geometry using the 514.5 nm line of an Ar^+ laser (Coherent 90C FreD), a power density on the sample surface of 1.4 kW/mm^2, acquisition times varying between 15 and 30 s and averaging over ten loops. The achieved spectral resolution was 2 cm^{-1}. Polarized spectra were collected on cooling from 850 to 80 K using a Linkam THMS-E600 stage with a cooling rate of 10 K/min and a temperature accuracy of ±0.1 K in $\bar{Z}(XX)Z$ and $\bar{Z}(XY)Z$ scattering geometries (Porto's notation), where X, Y, and Z are along the cubic [100], [010], and [001] crystallographic directions, respectively. Raman spectra at high pressures were conducted with a gas-membrane-driven easyLab Diacell® μScopeDAC-RT(G) diamond-anvil cell, using a 16:3:1 methanol-ethanol-water mixture as a pressure-transmitting medium, which is hydrostatic up to 10.5 GPa.[30] The pressure was determined by the ruby-line photoluminescence method[29] with an accuracy of 0.1 GPa. All measured spectra were reduced by the Bose-Einstein phonon occupation factor to eliminate the effect of temperature on the peak intensities and fitted with Lorentzian functions to determine the peak positions, full widths at half-maximums (FWHMs), and intensities. The intensities were further normalized to the corresponding total spectrum profile areas.

The reversibility of the observed temperature- or pressure-induced structural changes was verified by measurements at ambient conditions performed after the corresponding *in situ* experiments.

III. RESULTS AND DISCUSSION

A. The structural state at ambient conditions

The chemical analysis shows that in both PST-La and PSN-La the Sc/Ta ratio is considerably larger than unity and that there are some Pb vacancies. These effects result from the aliovalent substitution on the A site and they are more

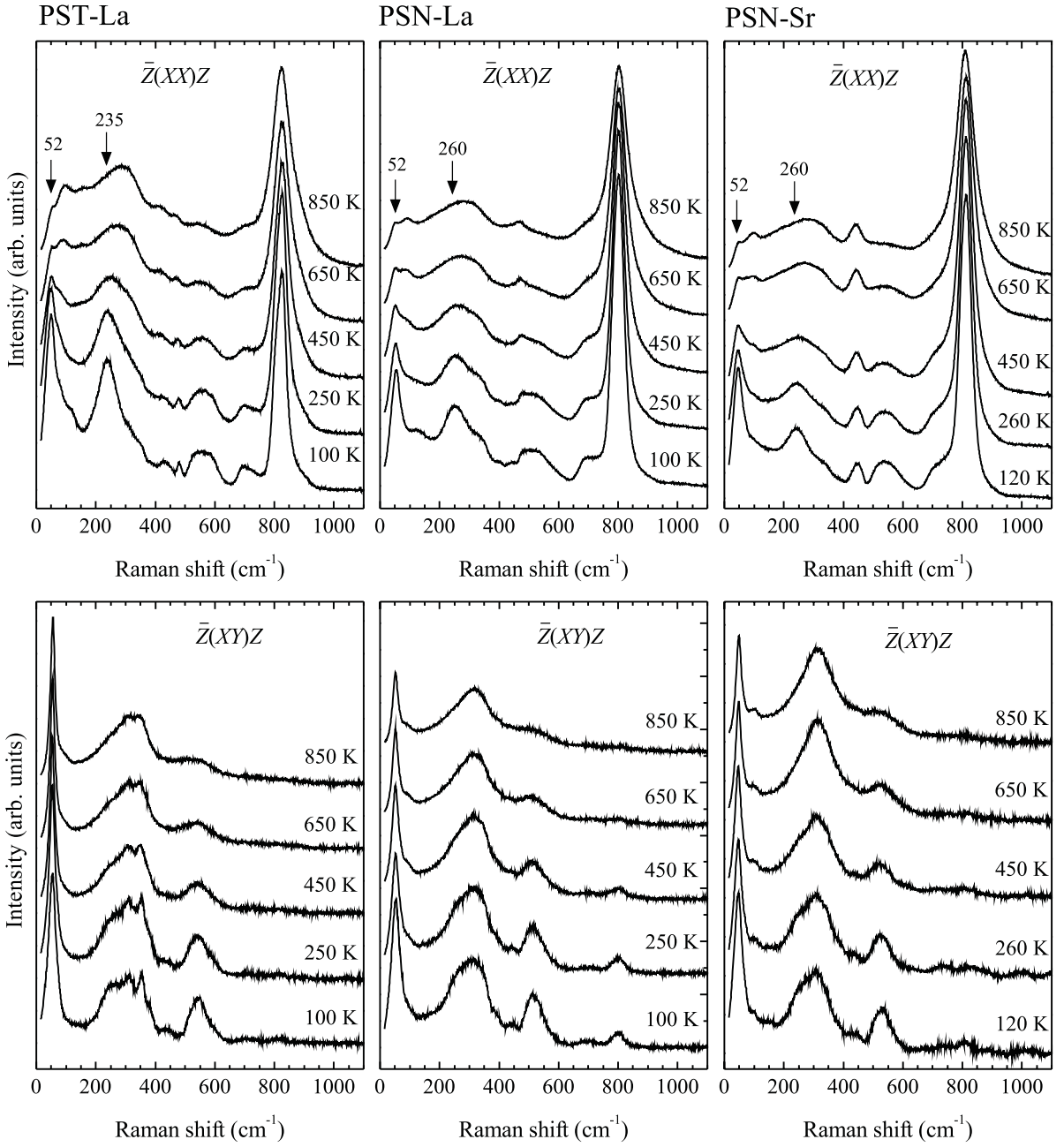

FIG. 2. Polarized $\bar{Z}(XX)Z$ and $\bar{Z}(XY)Z$ Raman spectra of PST-La, PSN-La, and PSN-Sr measured at different temperatures and ambient pressure.

pronounced for PSN-La compared to PST-La due to the larger content of La incorporated into the structure of the former sample. The calculated tolerance factor t for PST-La is 0.942 when the Pb vacancies are taken into account and 0.971 if the approximate formula $Pb_{1-x}La_xSc_{(1+x)/2}Ta_{(1-x)/2}O_3$, $x = 0.08$, is considered (see Table I). The corresponding t values for PSN-La are 0.926 and 0.961. As can be seen, even if the vacancies on the A site are neglected, the tolerance factors for the La-doped compound are smaller than the tolerance factors of the undoped compounds $t = 0.977$ [r_i(Ta) = r_i(Nb) = 0.64 Å [19]]. The tolerance factor for PSN-Sr is 0.971, also smaller than the tolerance factor of the undoped compound.

The powder XRD patterns of PSN-La and PSN-Sr did not reveal any superlattice Bragg reflections indicating a doubling of the perovskite-type structure, which is usually attributed to long-range 1:1 chemical ordering on the B site. The XRD pattern of PST-La exhibited very weak but relatively sharp superlattice Bragg peaks. By applying the Scherrer equation to the FWHM of the 111 Bragg peak (Miller indices throughout the whole paper refer to $Fm\bar{3}m$), the average size of regions generating the superlattice peaks with h,k,l, all odd is determined to be 45 nm. Assuming that the doubling of the structure is due to chemical 1:1 B-site order and using the intensity ratio between the superlattice and lattice Bragg

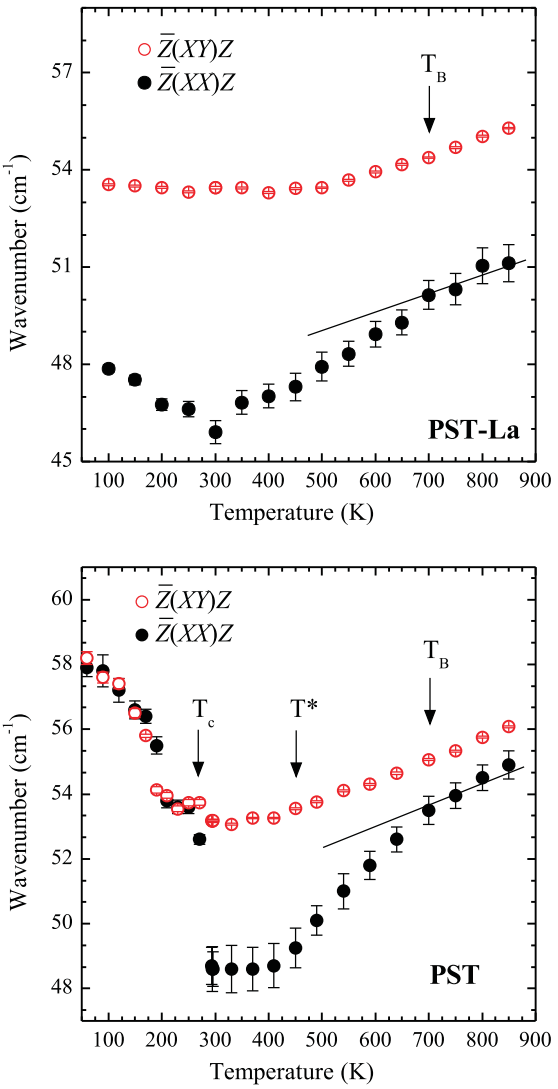

FIG. 3. (Color online) Temperature dependence of the positions of the Raman peaks related to the Pb-localized mode observed in $\bar{Z}(XX)Z$ (solid circles) and $\bar{Z}(XY)Z$ (open circles) geometry for PST-La (upper plot) and pure PST (bottom plot). The lines represent the linear fits of the wave numbers for the corresponding $\bar{Z}(XY)Z$ peaks in the temperature range above 500 K; T_c denotes the para-to-ferroelectric phase transition observed for PST.[6,41]

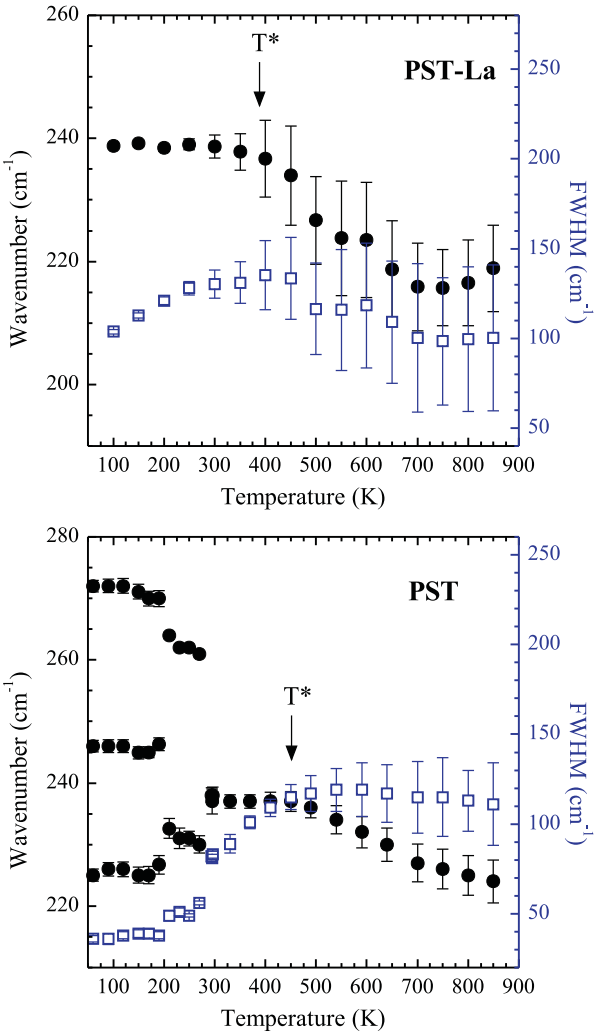

FIG. 4. (Color online) Temperature dependence of the position (solid circles) and the FWHM (open squares) of the Raman peak near 250 cm^{-1} observed in $\bar{Z}(XX)Z$ geometry for PST-La (upper plot) and pure PST (bottom plot). The peak splitting observed for PST below 280 K is due to the development of a ferroelectric phase and a further lowering of the rotational symmetry;[6] the FWHM below is given for the most intense component.

reflections,[36] the degree of 1:1 *B*-site order can be estimated to be 0.05. The actual degree of chemical order might be a bit different because of the difference between the atomic form factors of La and Pb.

In Fig. 1 the Raman spectra of PST-La, PSN-La, and PSN-Sr measured at room temperature and ambient pressure are compared with the corresponding spectra of the undoped compounds. Detailed analysis and assignment of the peaks observed in the spectra of Pb-based relaxors is given in Refs. 37 and 38. Here we will focus mainly on the effect of La on the local structure and dynamics. A striking result is that La doping suppresses the peak arising from Pb-BO_3 translations in PNRs, which appears near 135 and 150 cm^{-1} for PST and PSN, respectively. A suppression of this peak has only previously been observed under pressure and it occurs near p^*, at which pressure anti-phase BO_6 tilt order begins to develop. The corresponding Raman peak is also suppressed in the spectrum of PSN-Sr, indicating that this is a "strain" effect rather than a "charge" effect. Furthermore, the peak near 135 or 150 cm^{-1} is not suppressed in the spectra of Ba-doped PST or PSN (Refs. 6 and 18) measured at ambient pressure, indicating that the doping-induced decrease in the tolerance factor is the main reason for this change. The peak arising from off-centered *B*-site cations in PNRs (near 235 cm^{-1} for PST and near 260 cm^{-1} for PSN) is also less intense for the La- and Sr-doped compounds as compared to the undoped compounds. The suppression of the Raman signals related to off-centered cation displacements (near 135–150 and 235–260 cm^{-1}) indicates that the polar order is disturbed due to the replacement of Pb^{2+} by cations with a smaller ionic radius. This is in accordance with the results

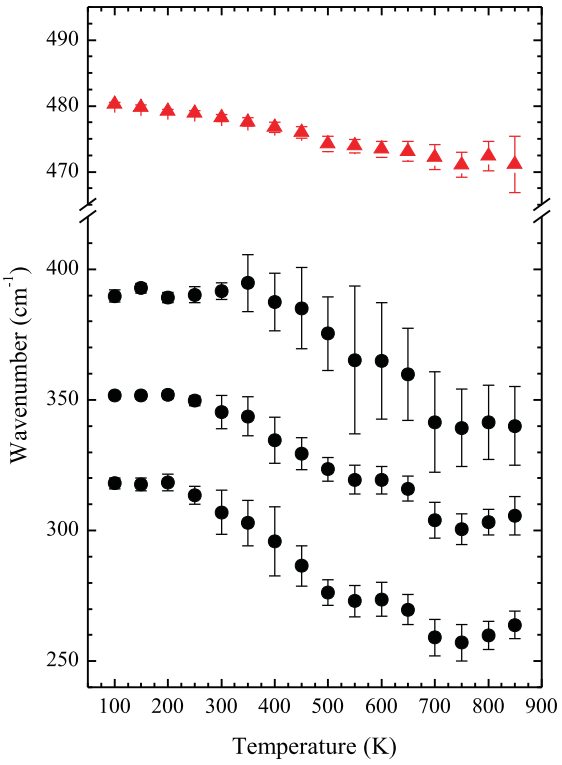

FIG. 5. (Color online) Temperature dependence of the positions of the Raman signals related to Pb-O bond-stretching modes (circles) and the position of the peak near 475 cm^{-1} (triangles) directly related structural species in the vicinity of La^{3+} measured for PST-La in $\bar{Z}(XX)Z$ geometry.

from resonance Raman spectroscopy, revealing smaller local polarizations and mean sizes of PNRs for La- and Sr-doped PSN.[39] On the other hand, in perovskite-type structures the octahedral tilting is favored by the smaller tolerance factor as well as by the absence of polar displacements of the cations. Hence, one might expect BO_6 tilting in La- and Sr-doped PST and PSN even at ambient pressure, although the Raman spectra alone cannot give unambiguous evidence for this. The additional weak peaks near 385–397 cm^{-1} in the doped samples are most probably due to the disturbance of the Pb-O-Pb linkages in the planes parallel to the cubic {111} planes, since the spectral range 300–360 cm^{-1} arises from Pb-O bond stretching modes.[37,38] The additional peak near 100 cm^{-1} reflects the doping-induced disturbance of the Pb system. Such a peak is not resolved in the spectrum of PST-La, probably due to the lower content of dopant in this compound. Only for the La-doped samples are the $\bar{Z}(XX)Z$ peak near 820 cm^{-1} and the $\bar{Z}(XY)Z$ peak near 550 cm^{-1} shifted to lower wave numbers. These peaks arise from internal BO_6 modes, symmetrical stretching and bending, respectively, and the peak shifts indicate that the strength of average *B*-O interactions weakens upon La doping. The effect is probably due to the increase in the B^{3+}/B^{5+} ratio induced by the incorporation of three-valent *A*-site cations. An additional peak at 475 cm^{-1} is observed in the $\bar{Z}(XX)Z$ spectra of both PST-La and PSN-La. This Raman signal is directly related to the presence of La^{3+} and thus is indicative of the atomic environment of the La cations, because the corresponding additional peak in the spectrum of PSN-Sr is observed near 445 cm^{-1}. The spectral range 400–500 cm^{-1} is dominated by BO_6 bending modes. Therefore, the doping-induced Raman peaks in this range are probably caused by modified BO_6 bending vibrations of those oxygen atoms that are shared between the *A*-site dopant and *B* cations. We assume that the doping-induced peak is positioned at a higher wave number in the case of La^{3+} as compared to Sr^{2+} incorporation because of the additional electrostatic term in the local potential associated with the higher charge.

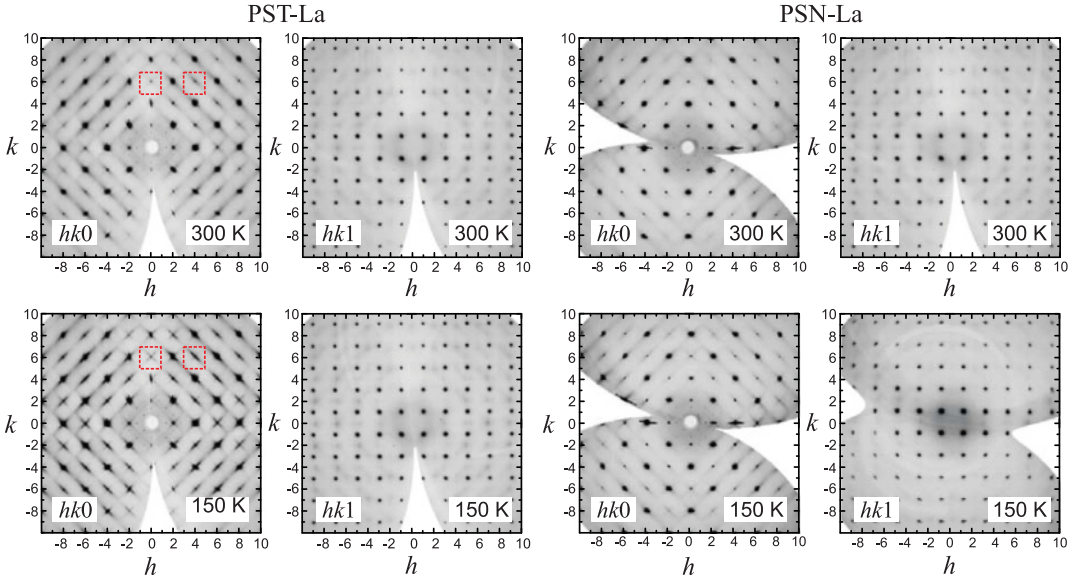

FIG. 6. (Color online) Reciprocal-space layers for PST-La and PSN-La, reconstructed from synchrotron single-crystal XRD data measured at different temperatures and ambient pressure (indices in $Fm\bar{3}m$). The dashed squares in the *hk*0 layer of PST-La indicate the areas shown in Fig. 7 on an enlarged scale.

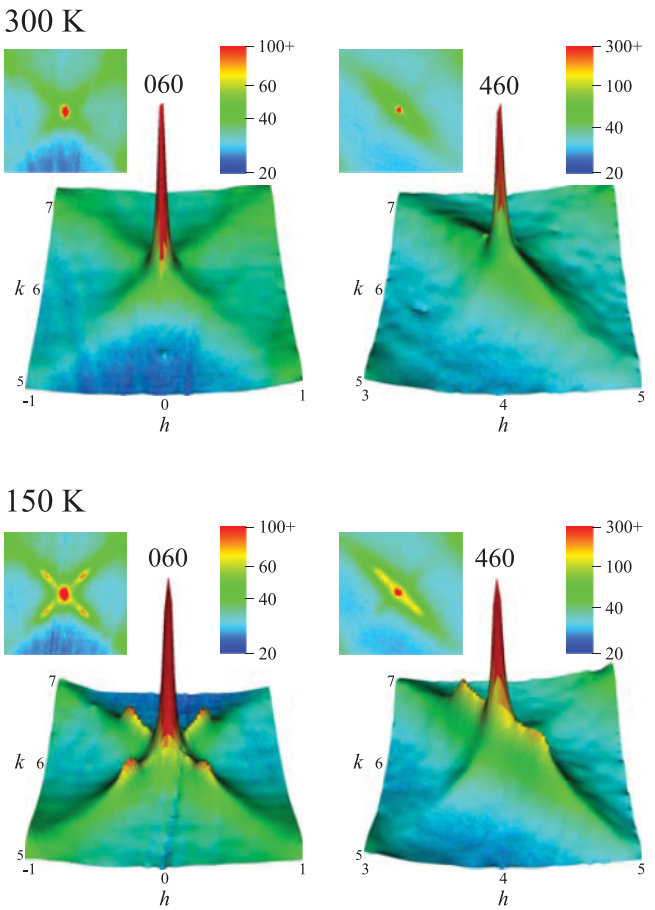

FIG. 7. (Color online) 3D and 2D view of the reflections 060 and 460 of PST-La at 150 and 300 K (indices in $Fm\bar{3}m$); the vertical scale in the 3D images is logarithmic.

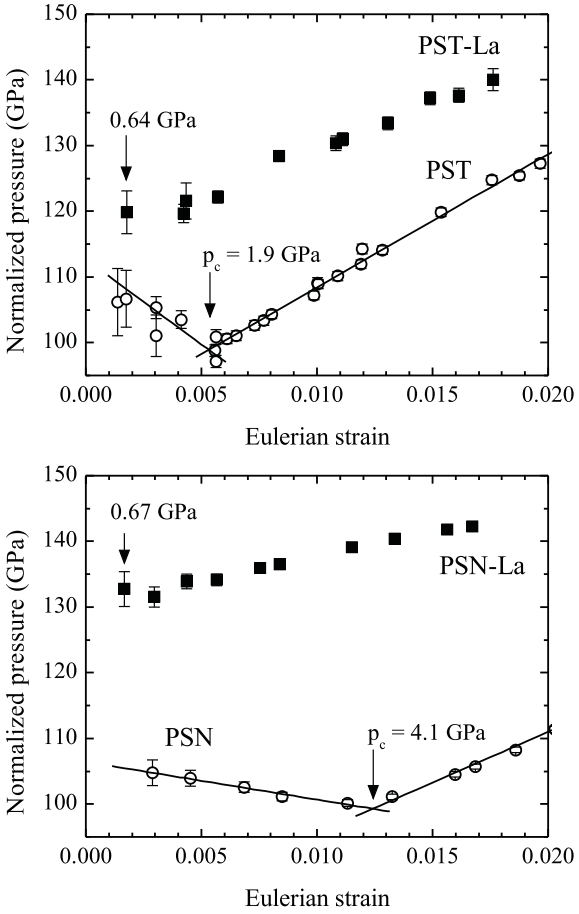

FIG. 8. Normalized pressure $F = p/3f(1+2f)^{5/2}$ versus the Eulerian strain $f = [(V_0/V)^{2/3} - 1]/2$ for La-doped (solid squares) and pure (open circles) PST (upper plot) and PSN (bottom plot), calculated from p-V experimental data sets.

B. Structural changes when temperature is the thermodynamic variable

The parallel $\bar{Z}(XX)Z$ and cross $\bar{Z}(XY)Z$ polarized Raman spectra measured at ambient pressure and different temperatures are shown in Fig. 2. For both La-doped compounds the temperature decrease does not substantially influence the intensity ratio between the Raman scattering observed in the cross polarized spectrum and the corresponding signal in the parallel polarized spectrum (compare, for example, the Raman intensity near 800 cm^{-1} in the two experimental geometries). The preservation of the depolarization ratio $\rho(\omega) = I_{XY}(\omega)/[I_{XX}(\omega) + I_{XY}(\omega)]$ at low temperatures indicates the absence of abundant long-range ordered rhombohedral domains. The same effect is observed for PSN-Sr as well as for Ba-doped PST and PSN.[6,18] Only in the case of Bi^{3+} does the A-site doping enhance the fraction of ferroelectric domains.[18] Therefore, the results presented here confirm that local elastic fields associated with substitutional disorder play an important role in the suppression of ferroelectric long-range order. Similar to other relaxors,[5,6] on cooling, the coupling between polar cation shifts is enhanced and consequently, the PNRs become larger. This is clearly indicated by the increase in the intensity of the Raman scattering near 250 cm^{-1} which is related to off-centered B-site cations and the $\bar{Z}(XX)Z$ peak near 52 cm^{-1} resulting from off-centered Pb ions.[37,38] It has previously been shown that the temperature evolution of phonon anomalies can reveal the characteristic temperatures T_B and T^*.[5,6,38] The uncertainties in the spectral parameters obtained by fitting were rather large for PSN-La and PSN-Sr because of the substantial peak overlaps in the range 100–400 cm^{-1} and hence we will discuss here only the trends for PST-La. Figure 3 shows the temperature dependence of the position ω of the Raman scattering near 52 cm^{-1} for pure and La-doped PST. The Raman scattering near 52 cm^{-1} is related to the Pb-localized F_{2g} mode of the prototype $Fm\bar{3}m$ structure, which is symmetry allowed in $\bar{Z}(XY)Z$ geometry and symmetry forbidden in $\bar{Z}(XX)Z$ geometry.[37] The appearance of anomalous $\bar{Z}(XX)Z$ Raman scattering near 52 cm^{-1} is due to the presence of polar shifts of Pb^{2+} cations. The Burns temperature T_B can be deduced from the deviation of the "anomalous" peak from the linear trend of the "allowed" peak associated with the Pb-localized vibrations.[6] As can be seen in Fig. 3, La doping does not change T_B. However, La doping modifies the structural transformations on further cooling. Only a minimum near 300 K in the $\omega_{XX}(T)$ is observed for PST-La, instead of a plateaulike dependence between T^* and T_c for PST. The intermediate temperature T^* can be revealed from the drop in the FWHM of the peak near 250 cm^{-1} (Refs. 6 and 7) related

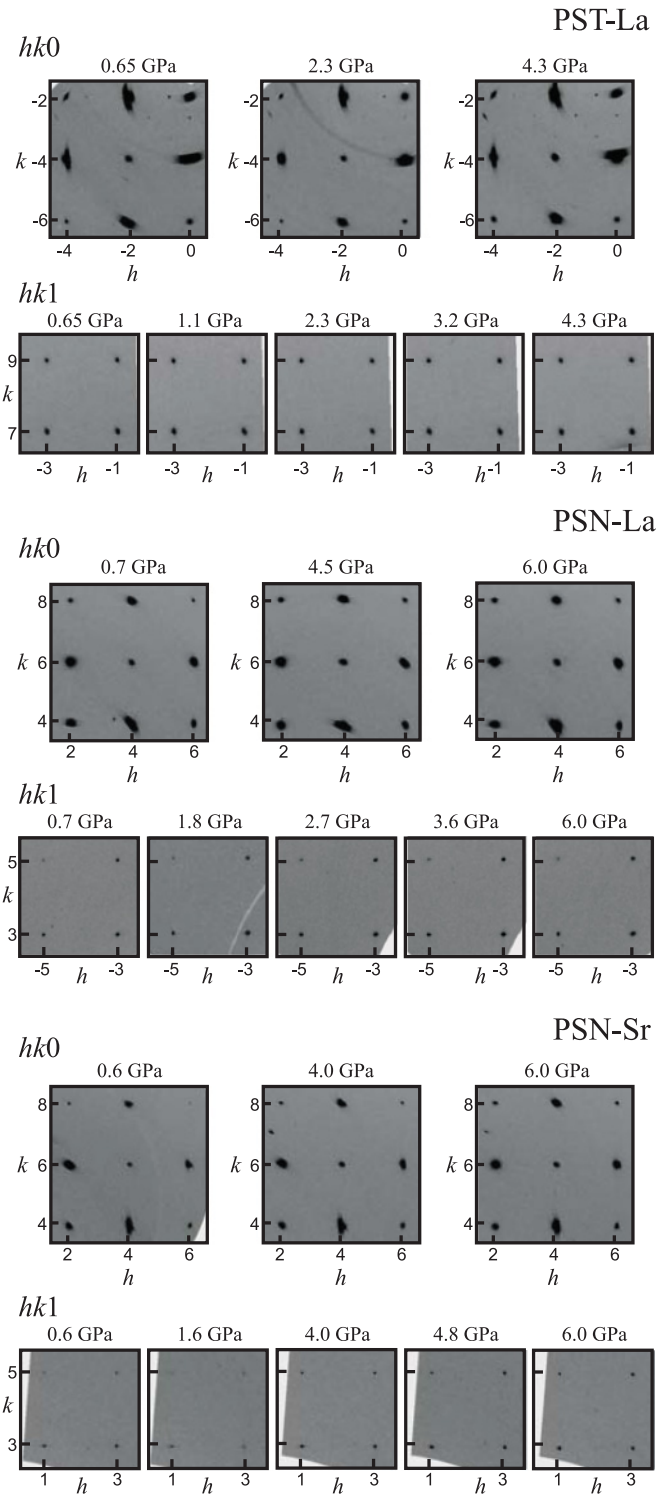

FIG. 9. *hk*0 and *hk*1 layers (indices in $Fm\bar{3}m$) of PST-La, PSN-La, and PSN-Sr reconstructed from high-pressure synchrotron single-crystal XRD data.

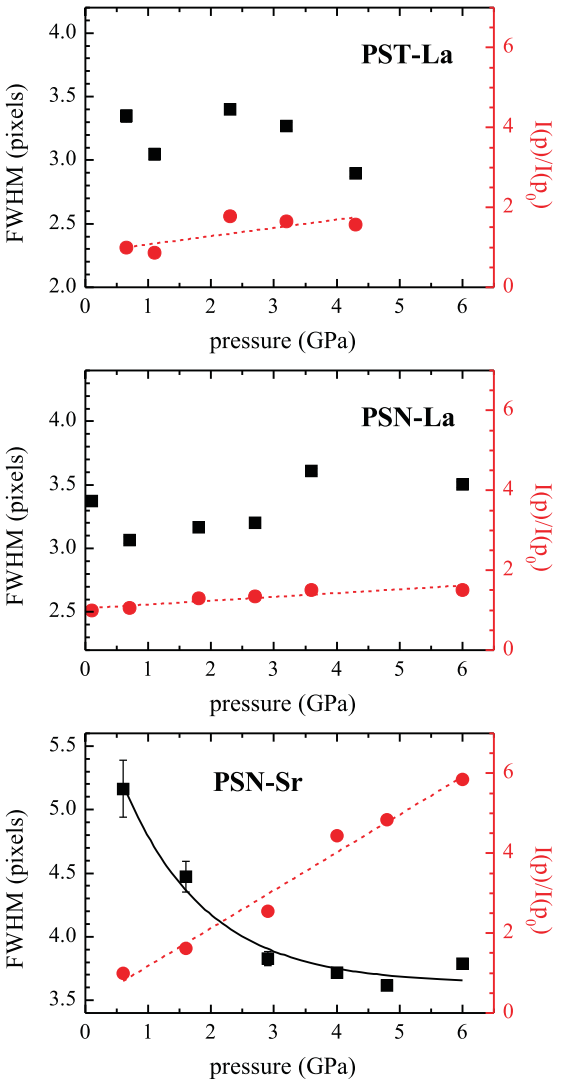

FIG. 10. (Color online) Pressure dependence of the FWHM and normalized integrated intensities of representative Bragg reflections determined by fitting the corresponding line profiles perpendicular to the direction of the ⟨100⟩* x-ray diffuse scattering with Gaussian functions. The evaluated Bragg peaks are $\bar{5}91$ for PST-La, $\bar{3}31$ for PSN-La, and 531 for PSN-Sr. The dashed lines represent linear fits to the corresponding data sets; the solid line in the bottom plot represents an exponential-decay fit to the FWHM data for PSN-Sr.

to the *B*-cation-localized F_{1u} mode of the prototype $Fm\bar{3}m$ structure. This mode is infrared active and its Raman activity is due to the presence of polar shifts of B-site cations.[37,38] For PST the $\omega(T)$ dependence of peak near 250 cm^{-1} reaches a saturation at T^*.[6] As can be seen in Fig. 4, La doping decreases T^* by approximately 60 K. This also indicates that the incorporation of La disturbs the temperature-driven polar order. Figure 5 compares the temperature dependence of the Raman peaks related to Pb-O bond-stretching modes[37,38] and the peak near 475 cm^{-1} directly related to the presence of La. At low temperatures the Raman signals arising from Pb-O bond-stretching modes reach saturation, whereas the peak near 475 cm^{-1} just increases in wave number with temperature decrease. This indicates that oxygen nearest neighbors of La are not involved in temperature-driven transformation processes and La^{3+} should be considered as only a modifier of the Pb system.

The two La-doped samples were also studied by synchrotron single-crystal XRD at two different temperatures (see Fig. 6). Similar to all Pb-based perovskite-type relaxors,[3,42,43] PST-La and PSN-La exhibit x-ray diffuse scattering along

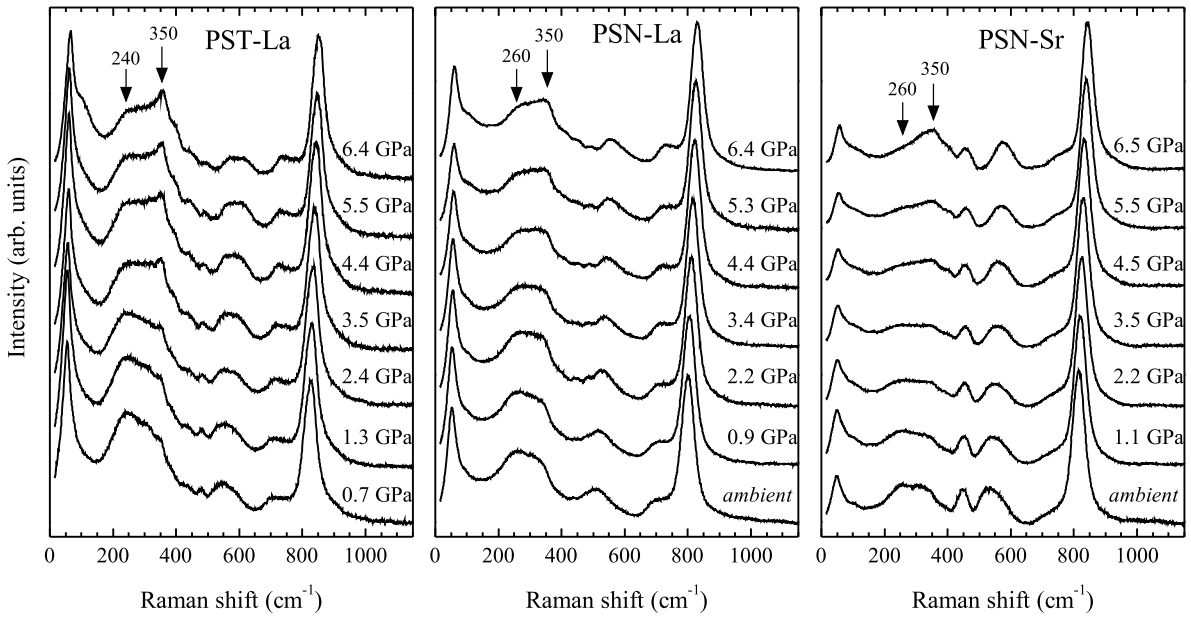

FIG. 11. Unpolarized Raman spectra of PST-La, PSN-La, and PSN-Sr measured at different pressures and room temperature.

$\langle 110 \rangle^*$, which arises from the off-centered cation displacements in PNRs.[42,43] The $\langle 110 \rangle^*$ x-ray diffuse scattering increases on cooling, indicating that the fraction of PNRs becomes larger. For PST-La additional satellite peaks were observed around the Bragg reflections in the $hk0$ layer at 150 K (Figs. 6 and 7) at approximately $\pm a^*/4, \pm a^*/4, 0$ from the Bragg positions. Such satellites have been observed previously by electron diffraction from single crystals of PST with a very high degree (>0.9) of chemical B-site order,[44] and were attributed to incommensurate modulations of the antiferroelectric order of Pb ions[44] on the basis of Monte Carlo simulations. We propose that PST-La also develops frustrated anti-ferroelectric Pb order on cooling. Since the satellite peaks in PST-La were detected by XRD, the length of coherence of the antipolar shifts of the Pb ions in PST-La should be larger than that in pure PST. The antiferroelectric Pb order in PST is supported by the high degree of chemical 1:1 B-site order because the latter doubles the structure in such a way that facilitates the antiferroelectric order of the Pb ions.[44] The PST-La crystals studied here are in fact chemically B-site disordered (approximate degree of order 0.05). Therefore, chemical B-site order cannot be the reason for the structural doubling that supports the antiferroelectric order of Pb developed at low temperatures. Our Raman-scattering data (see Fig. 1) indicate that at ambient pressure the structural state of the La-doped PST and PSN resembles the high-pressure structural state of pure PST and PSN. Under pressure Pb-based relaxors develop antiphase octahedral tilting,[14,15] which also leads to doubling of the unit-cell repeats of the perovskite structure. Hence, in the case of La-doped PST the existence of long-range BO_6 tilt order at room temperature and ambient pressure may be the true factor supporting the frustrated antferroelectric order of Pb that evolves on cooling. Antiphase octahedral tilting at ambient pressure and room temperature should also be characteristic of PSN-La. However, antiferroelectric order of Pb was not observed for PSN-La, most probably because the content of La in this compound is so high that it dilutes the interactions between the Pb ions so that coherent domains with Pb order large enough to be detected by XRD do not develop. The $hk1$ layers for both PST-La and PSN-La show rather intense odd-odd-odd spots. From our experience with other Pb-based relaxors with a low degree of chemical B-site order,which were probed by in-house powder XRD and single-crystal synchrotron XRD using the same instrumentation and experimental conditions as for PST-La and PSN-La,[6,18,38,40] the La-doped compounds exhibit surprisingly strong odd-odd-odd peaks detected by single-crystal synchrotron XRD, suggesting that the odd-odd-odd spots in the $hk1$ layers may result from antiphase octahedral tilt order or at least may be a combined effect of chemical B-site order and antiphase BO_6 tilt order. To verify this assumption we have conducted *in situ* high-pressure experiments.

C. Structural changes when pressure is the thermodynamic variable

Figure 8 shows the normalized pressure $F = p/[3f(1+2f)^{5/2}]$ as a function of the pressure-induced Eulerian strain $f = [(V_0/V)^{2/3} - 1]/2$ for pure and La-doped PST and PSN, calculated from the pressure dependence of the unit-cell volume V determined by single-crystal XRD. When the Gibbs free energy of the crystal is expanded in a Taylor series up to the third term in the strain (the Birch-Murnaghan third-order EoS), the derivative dF/df is proportional to $K_0(K_0' - 4)f$, where $K_0 = -V(dp/dV)_{p=0}$ is the ambient-pressure bulk modulus and $K_0' = (dK/dp)_{p=0}$. Therefore, a change in the $F(f)$ slope indicates a discontinuity in K_0 or K_0', or both, and hence reveals the occurrence of a phase transition. As can be seen in Fig. 8, pure PST and PSN undergo a phase transition at 1.9 GPa and 4.1 GPa, respectively. Above the critical pressure dF/df is positive. For both PST-La and PSN-La the $F(f)$ slope is already positive above 0.7 GPa. Given the fact that antiphase tilting evolves at p^*, which for pure PST and PSN is at least 0.7 GPa below p_c,[14,15] the f-F data strongly support the conclusion that

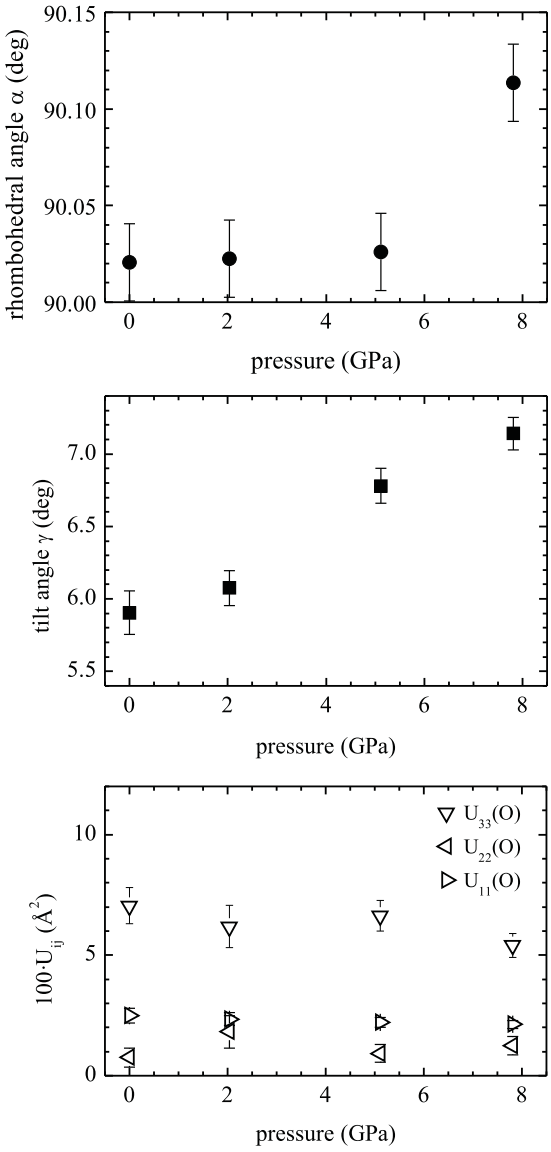

FIG. 12. Rhombohedral unit-cell angle α (solid circles), tilt angle $\gamma = [180 - \angle(\mathrm{BOB})]/2$ (solid squares) and oxygen atomic displacement parameters (open symbols) obtained from Rietveld refinements to powder neutron diffraction on PSN-La performed in $R\bar{3}c$. Refinements in *I*4/*mcm* and *Imma*, which are also consistent with antiphase octahedral tilts, yielded unsatisfactory fits.

in PST-La and PSN-La antiphase tilts are already ordered at ambient pressure.

The *hkl* layers of PST-La, PSN-La, and PSN-Sr reconstructed from high-pressure synchrotron single-crystal XRD data are shown in Fig. 9. For all three compounds the x-ray diffuse scattering along $\langle 110 \rangle^*$ is suppressed at 0.7 GPa. A pressure-induced suppression of the $\langle 110 \rangle^*$ x-ray diffuse scattering is typical of all Pb-based relaxors[10,12,13,38,45,46] but it happens above the critical pressure. The odd-odd-odd Bragg reflections are sharp for all three compounds. For PSN-La and PSN-Sr the odd-odd-odd peaks at low pressures are accompanied by x-ray diffuse scattering along $\langle 100 \rangle^*$. Such pressure-induced diffuse scattering was also observed for other Pb-based relaxors.[14,38,47] The $\langle 100 \rangle^*$ diffuse scattering is most probably due to intermediate-range order of octahedral tilts, since it disappears at higher pressures. For PSN-Sr the FWHM of the odd-odd-odd peaks decreases with pressure, while the intensity gradually increases (see Fig. 10), as in the case of other Pb-based relaxors.[13,14,38] For PST-La and PSN-La the odd-odd-odd Bragg peaks are sharp even at 0.7 GPa and their widths and intensities do not change substantially with pressure, indicating that the pressure-induced structural changes detectable via XRD are weak. Raman spectroscopy, however (see Fig. 11), clearly shows that all three compounds studied here exhibit the same pressure-induced structural changes that have been already observed for other Pb-based relaxors:[10,12,13,38,45,46] a reduction of off-centered *B*-site cations as indicated by the suppression of the peak near 250 cm^{-1} and an enlargement of ferroic Pb-O species as indicated by the enhancement of the Raman scattering near 350 cm^{-1}.[10,12,13,48] It should be noted that the suppression of the peak near 250 cm^{-1} is less pronounced for the La-doped compounds as compared to the Sr-doped compound. Therefore, the local electric fields associated with La^{3+} must oppose the effect of external pressure in suppressing the preexisting polar *B*-cation shifts. Rietveld refinements to powder neutron-diffraction data on PSN-La unambiguously revealed that the structure at ambient conditions has a rhombohedral metric and includes considerable BO_6 tilting (see Fig. 12), which is typical of the high-pressure phase of Pb-based relaxors.[14,15] Neutron-diffraction analysis also clearly showed that the octahedral tilting increases with pressure. It should be mentioned that the results presented in Fig. 12 were obtained in space group $R\bar{3}c$ assuming isotropic Pb atomic displacement parameters $U_{ij} = U_{\mathrm{iso}}$, $i = j = 1,2,3$. Structure refinements in $R\bar{3}c$ with anisotropic Pb atomic displacement parameters, $U_{11} = U_{22} < U_{33}$ as in the case of PST and PST-Ba (Ref. 14) or $U_{11} = U_{22} > U_{33}$ as in the case of PSN,[15] yielded almost the same values for goodness-of-fit and tilt angles, but in both cases the values of the smaller U_{ii} were negative. Variations of the occupation factors in both the *A* and *B* sites (to account for plausible deviations in the chemistry as determined by electron microprobe analysis) as well as the use of isotropic U_{ij} for La and anisotropic U_{ij} for Pb could not overcome the physically meaningless negative U_{ij} values for Pb. Since the oxygen U_{ij} refined in $R\bar{3}c$ were anisotropic (Fig. 12) we also performed Rietveld refinements in a space group of lower symmetry, $R3c$, releasing the oxygen atom shifts in all three directions. In this case the refined U_{ij} of the Pb cations were anisotropic and positive but the goodness-of-fit was significantly worsened. Since the refined tilt angle in all cases was nearly the same, we have chosen the simplest model of $R\bar{3}c$ with average isotropic atomic displacement parameters on the *A* site. This is also physically consistent with the fact that 23% of Pb cations are replaced by La, which has no stereochemically active lone-pair electrons, and that at ambient pressure a doping-induced tilting occurs, which reduces the volume of oxygen cavity around Pb and thus the off-centered local displacements of Pb cations. Therefore, the overall off centering of the *A*-site cations is expected to be smaller for PSN-La as compared to PST, PST-Ba, and PSN, and this is probably also the reason we are unable to resolve anisotropy in the corresponding atomic displacement parameters.

The similarity between PST-La and PSN-La regarding the $F(f)$ dependence and the pressure evolution of the Raman

scattering indicates that these structural features are also characteristic of PST-La. The refinements to the neutron-diffraction data show that for PST, PST-Ba, and PSN the tilt angle increases from zero to ∼8°, 4°, and 7°, respectively, over a pressure range of ∼5 GPa.[14,15] For PSN-La the tilt angle is already 5.9° at ambient pressure and up to 7.8 GPa it only increases by 1.2°. This small change in the tilt angle explains the lack of variation in the intensities of the odd-odd-odd Bragg peaks in the synchrotron XRD patterns of the La-doped compounds (Fig. 10). The comparison between the trends in the XRD peaks for La- and Sr-doped relaxors (Fig. 10) suggests that in PSN-Sr the degree of BO_6 tilt order at ambient pressure is lower than in PST-La and PSN-La. This is most probably due to the fact that the doping-induced decrease in the tolerance factor is smaller for Sr than for La.

IV. CONCLUSIONS

Our study reveals that the incorporation of La^{3+} in the relaxor structure strongly disturbs the dynamical coupling between off-centered Pb and *B*-site cations and enhances antiphase BO_6 octahedral tilting at ambient conditions. The former is due to the partial violation of the lone-pair system, while the latter arises from the decrease in the tolerance factor. These structural changes facilitate antipolar coupling between Pb^{2+} ions and, depending on the *A*-site doping level, frustrated antiferroelectric order of Pb^{2+} ions detectable by XRD can be developed at low temperatures. The results presented here underline the importance of doping-induced strain effects versus charge effects *even in the case of aliovalent doping*. The strain effects might play a significant role for the La-doping-induced crossover from a normal-ferroelectric to a relaxor state in $PZ_{1-x}Ti_xO_3$. The results presented here further highlight the importance of random local elastic strains for the nanoscale ferroic order in complex perovskite-type crystals.

ACKNOWLEDGMENTS

Financial support by the Deutsche Forschungsgemeinschaft (MI 1127/2-2, INST 152/460-1, and INST 152/526-1), National Science Foundation (EAR-0738692), and the Bulgarian Ministry of Science and Education (BY-X-308) is gratefully acknowledged. Experiments at the ISIS Pulsed Neutron and Muon Source were supported by a beamtime allocation from the Science and Technology Facilities Council and the EU funded NMI3 programme.

*Corresponding authors: bernd.maier@mineralogie.uni-hamburg.de;
†boriana.mihailova@uni-hamburg.de

[1] L. E. Cross, Ferroelectrics **76**, 241 (1987).
[2] A. A. Bokov and Z. G. Ye, J. Mater. Sci. **41**, 31 (2006).
[3] G. Xu, J. Phys. Soc. Jpn. **79**, 011011 (2010).
[4] G. Burns and B. A. Scott, Solid State Commun. **13**, 423 (1973).
[5] J. Toulouse, F. Jiang, O. Svitelskiy, W. Chen, and Z. G. Ye, Phys. Rev. B **72**, 184106 (2005).
[6] B. Mihailova, B. Maier, C. Paulmann, T. Malcherek, J. Ihringer, M. Gospodinov, R. Stosch, B. Güttler, and U. Bismayer, Phys. Rev. B **77**, 174106 (2008).
[7] B. Dkhil, P. Gemeiner, A. Al-Barakaty, L. Bellaiche, E. Dul'kin, E. Mojaev, and M. Roth, Phys. Rev. B **80**, 064103 (2009).
[8] J.-H. Ko, D. H. Kim, and S. Kojima, Appl. Phys. Lett. **90**, 112904 (2007).
[9] E. Dul'kin, B. Mihailova, M. Gospodinov, M. E. Mojaev, and M. Roth, J. Phys. Condens. Matter **22**, 222201 (2010).
[10] B. Mihailova, R. J. Angel, A.-M. Welsch, J. Zhao, J. M. Engel, C. Paulmann, M. Gospodinov, H. Ahsbahs, R. Stosch, B. Güttler, and U. Bismayer, Phys. Rev. Lett. **101**, 017602 (2008).
[11] A.-M. Welsch, B. Mihailova, R. Stosch, B. Güttler, M. Gospodinov, and U. Bismayer, J. Phys. Condens. Matter **21**, 235901 (2009).
[12] A.-M. Welsch, B. J. Maier, J. M. Engel, B. Mihailova, R. J. Angel, C. Paulmann, M. Gospodinov, A. Friedrich, R. Stosch, B. Güttler, D. Petrova, and U. Bismayer, Phys. Rev. B **80**, 104118 (2009).
[13] B. J. Maier, A.-M. Welsch, R. J. Angel, B. Mihailova, J. Zhao, J. M. Engel, L. A. Schmitt, C. Paulmann, M. Gospodinov, A. Friedrich, and U. Bismayer, Phys. Rev. B **81**, 174116 (2010).
[14] B. J. Maier, R. J. Angel, W. G. Marshall, B. Mihailova, C. Paulmann, J. M. Engel, M. Gospodinov, A.-M. Welsch, D. Petrova, and U. Bismayer, Acta Crystallogr., Sect. B: Struct. Sci. **66**, 280 (2010).
[15] B. J. Maier, R. J. Angel, B. Mihailova, W. G. Marshall, M. Gospodinov, and U. Bismayer, J. Phys. Condens. Matter **23**, 035902 (2011).
[16] N. Setter and L. E. Cross, J. Appl. Phys. **51**, 4356 (1980).
[17] G. A. Samara, E. L. Venturini, and L. A. Boatner, J. Appl. Phys. **100**, 074112 (2006).
[18] B. J. Maier, B. Mihailova, C. Paulmann, J. Ihringer, M. Gospodinov, R. Stosch, B. Güttler, and U. Bismayer, Phys. Rev. B **79**, 224108 (2009).
[19] R. D. Shannon and C. T. Prewitt, Acta Crystallogr., Sect. B: Struct. Sci. **25**, 925 (1969); R. D. Shannon, Acta Crystallogr., Sect. A: Cryst. Phys., Diffr., Theor. Gen. Crystallogr. **32**, 751 (1976).
[20] T. Okawa, M. Imaeda, and H. Ohsato, Mater. Sci. Eng., B **88**, 58 (2002).
[21] C. Laulhé, A. Pasturel, F. Huppert, and J. Kreisel, Phys. Rev. B **82**, 132102 (2010).
[22] Z. Xu, X. Dai, J.-F. Li, and D. Viehland, Appl. Phys. Lett. **68**, 1628 (1996).
[23] R. J. Angel and L. W. Finger, J. Appl. Cryst. **44**, 247 (2011).
[24] F. Craciun, Phys. Rev. B **81**, 184111 (2010).
[25] B.-G. Kim, S. M. Cho, T.-Y. Kim, and H. M. Jang, Phys. Rev. Lett. **86**, 3404 (2001).
[26] C. Paulmann and T. Malcherek, Hasylab Annual Report, Part I, 2006, p. 1399.
[27] R. Boehler, Rev. Sci. Instrum. **77**, 115103 (2006).
[28] H. Ahsbahs, Z. Kristallogr. **219**, 305 (2004).
[29] R. G. Munro, G. J. Piermarini, S. Block, and W. B. Holzapfel, J. Appl. Phys. **57**, 165 (1985).
[30] R. J. Angel, M. Bujak, J. Zhao, G. D. Gatta, and S. D. Jacobsen, J. Appl. Crystallogr. **40**, 26 (2007).

[31]R. Miletich, D. R. Allan, and W. F. Kuhs, in *High-Pressure Single-Crystal Techniques in High-Pressure and High-Temperature Crystal Chemistry*, edited by R. M. Hazen and R. T. Downs, Reviews in Mineralogy and Geochemistry Vol. 41 (Mineralogical Society of America, Washington, DC, 2000), pp. 445–520.

[32]R. J. Angel and L. W. Finger, J. Appl. Crystallogr. **44**, 247 (2011).

[33]R. J. Angel, D. R. Allan, R. Miletich, and W. L. Finger, J. Appl. Crystallogr. **30**, 461 (1997).

[34]B. H. Toby, J. Appl. Crystallogr. **34**, 210 (2001).

[35]A. C. Larson and R. B. von Dreele, *General Structure Analysis System (GSAS)*, Los Alamos National Laboratory Report LAUR 86-748 (2004).

[36]C. G. F. Stenger and A. J. Burggaaf, Phys. Status Solidi A **61**, 275 (1980).

[37]B. Mihailova, U. Bismayer, B. Güttler, M. Gospodinov, and L. Konstantinov, J. Phys. Condens. Matter **14**, 1091 (2002).

[38]A.-M. Welsch, B. J. Maier, B. Mihailova, R. J. Angel, J. Zhao, C. Paulmann, J. M. Engel, M. Gospodinov, V. Marinova, and U. Bismayer, Z. Kristallogr. **226**, 126 (2011).

[39]B. Mihailova, M. Bastjan, B. Schulz, M. Rübhausen, M. Gospodinov, T. Malcherek, R. Stosch, B. Güttler, and U. Bismayer, Appl. Phys. Lett. **90**, 042907 (2007).

[40]N. Waeselmann, B. Mihailova, B. J. Maier, C. Paulmann, M. Gospodinov, V. Marinova, and U. Bismayer (unpublished).

[41]E. Dul'kin, B. Mihailova, M. Catalan, M. Gospodinov, and M. Roth, Phys. Rev. B **82**, 180101(R) (2010).

[42]M. Paściak, M. Wołcyrz, and A. Pietraszko, Phys. Rev. B **76**, 014117 (2007).

[43]T. R. Welberry and D. J. Goossens, J. Appl. Crystallogr. **41**, 606 (2008).

[44]K. Z. Baba-Kishi and M. Paściak, J. Appl. Crystallogr. **43**, 140 (2010).

[45]B. Chaabane, J. Kreisel, B. Dkhil, P. Bouvier, and M. Mezouar, Phys. Rev. Lett. **90**, 257601 (2003).

[46]P. E. Janolin, B. Dkhil, P. Bouvier, J. Kreisel, and P. A. Thomas, Phys. Rev. B **73**, 094128 (2006).

[47]B. J. Maier, R. J. Angel, B. Mihailova, J. M. Engel, A.-M. Welsch, C. Paulmann, M. Gospodinov, and U. Bismayer, DESY annual report, 2009.

[48]J. Kreisel, B. Dkhil, P. Bouvier, and J.-M. Kiat, Phys. Rev. B **65**, 172101 (2002).